Mechanics of Advanced Composite Structures 11 (2024) 41 – 58

Semnan University

Mechanics of Advanced Composite Structures

journal homepage: http://MACS.journals.semnan.ac.ir

Nonlinear Torsional Vibration of Size-Dependent Functionally Graded Rods

R. Nazemnezhad *, E. Razavian Shad, A.A. Jandaghian

School of Engineering, Damghan University, Damghan, Iran

KEYWORDS

Torsional vibration;
Von-Kármán type nonlinearity;
Surface elasticity theory;
Internal resonances;
Multiple scale method.

ABSTRACT

This study aims to investigate the effect of functionally graded materials (FGMs) on the internal resonances of nanorods in torsional vibration. The von-Kármán type nonlinearity is considered and the governing equation of motion is derived using Hamilton's principle based on the surface elasticity theory. It is assumed that the properties of the functionally graded (FG) nanorod vary through the radius direction based on power-law distribution. Then, the multi-mode Galerkin method is implemented to convert the partial differential equation to an ordinary differential one. In the next step, the method of multiple scales is used to derive the natural frequencies as well as the conditions in which the internal resonances occur. The results are presented for two types of end conditions, fixed-fixed and fixed-free, and the effects of variations of various parameters like length, radius, and amplitude of vibration on natural frequencies are investigated. This research shows that functionally graded materials differ in the state of happening the internal resonances in the presence of the surface energy.

1. Introduction

Functionally graded materials (FGMs) are non-homogeneous materials made up by changing volume fractions of two (or more) various materials in the chosen spatial directions. The gradual change in materials results in an inhomogeneous composite with smooth and constant mechanical, electrical, and thermal properties. These variations remove inter-plane issues and lead to stress distribution with a smooth profile, upper fracture toughness, and better thermal resistance, which captured significant attention in numerous engineering applications. Due to these excellent properties, FG structures have been used in different engineering fields like mechanical, aerospace, chemical, and biomechanics. [1-13].

By growing in material fabrication and nanostructures, FG materials are increasingly used in many micro- and nano-applications such as micro/nano-electromechanical systems (M/NEMS), micro switches, and microelectronics [14-22]. In this matter, numerous experimental investigations have been done to study the mechanical behavior of micro and nanostructures [23-25]. The results from the experimental studies have shown that since classical continuum mechanics theories are not size-dependent, various novel continuum mechanics theories are needed to study nano-scaled structures and predict their behavior. Thus, to account for the intrinsic characteristics of materials at micro and nanostructures various theories have been suggested to explain the elastic behaviors of these micro and nano-scale systems such as surface elasticity theory, nonlocal elasticity theory, modified couple stress theory, and strain gradient theory. As surface energy is less significant than bulk energy at the macroscale, its effect is not taken into account. The surface effects become significant because nano-scaled objects have a high surface-to-volume ratio. Consequently, it is important to consider surface energy while doing a mechanical study of nanostructures. Gurtin et al. [26, 27] presented a mathematical theory for the accurate prediction of mechanical behaviors of nano-scaled structures to examine the impact of surface stress on the mechanics of

* Corresponding author. Tel./Fax: +98-23-35220414
E-mail addresses: rnazemnezhad@du.ac.ir; mrnazemnezhad@gmail.com

DOI: 10.22075/macs.2023.29907.1479
Received 2023-03-23; Received in revised form 2023-08-04; Accepted 2023-08-15

nanostructures. As a result, in recent years, the number of research reports on this subject dramatically grew [28-33].

Baron et al. developed a continuous model for nanobeams that takes into account both surface effects and material heterogeneity [34]. A theoretical model was presented by Wang and Feng to study the effects of surface elasticity and residual surface tension on the natural frequency of microbeams [35]. The Gurtin and Murdoch theory was used by Ansari and Sahmani to study the buckling and bending of nanobeams. From their work, explicit formulas for various beam theories were derived [36]. A modified continuum model was developed by Ansari et al. to predict the post-buckling deflection of nanobeams [37]. The generalized differential quadrature (GDQ) method was used to solve governing differential equations. Abbasion et al. [38] presented a comprehensive model to study how surface elasticity and residual surface tension affect the natural frequency of microbeam flexural vibrations when shear deformation and rotary inertia effects are considered. Based on the nonlocal elasticity theory, Wang presented an analytical model to predict surface effects on fluid-conveying nanotubes' free vibration [39]. Their findings showed that the surface effects with positive elastic constant or positive residual surface tension tend to increase critical flow velocity and the natural frequency. The influence of surface effects on the vibration of nanotubes was studied by Farshi et al. based on the Timoshenko beam model [40]. The influence of surface elasticity and surface stress on the static bending of nanowires was investigated by He and Lilley [41]. Three different boundary conditions i.e. clamped-free, simply supported, and clamped–clamped was taken into account using the Euler–Bernoulli beam theory. Civalek et al. studied the size-dependent stability analysis of restrained nanobeam with functionally graded material via nonlocal Euler–Bernoulli beam theory using the Fourier series [42]. Uzun and Yayli reformulated a new stability model for the nano-sized beam resting on a one-parameter elastic foundation. The stability solution was based on the nonlocal strain gradient elasticity theory [43].

In recent times, the influence of surface effect on the nonlinear free vibration behaviors of nanobeams has been done in some research. The nonlinear free vibration of nanobeams was investigated by Nazemnezhad et al. [44]. They considered surface effects and used Euler–Bernoulli beam theory. Based on the Gurtine-Murdoch continuum theory, the nonlinear free vibration behavior of Timoshenko nanobeams was studied by Ansari et al. [45]. Nonlinear free vibration of functionally graded nanobeams was studied by Asgharifard Sharabiani et al. using the Euler-Bernoulli beam theory [46]. Yayli investigated various points including buckling, thermal buckling, axial vibration, lateral vibration, and longitudinal vibration [47-53].

Torsional vibration becomes significant in some devices, such as nanoelectromechanical systems, nano-scaled shafts, and nano servomotors as nanotubes are exposed to external torques. Studies on the free torsional vibration of nanotubes are few. Lim et al. [54] developed a new elastic nonlocal stress model as well as analytical solutions for the torsional dynamics of circular nanorods/nanotubes. Free torsional vibration behaviors of nanotubes made of a bi-directional functionally graded (FG) material with properties that changed continuously along the radius and length directions investigated by Li and Hi [55]. Based on the nonlocal elasticity theory, Murmu et al. [56] examined the torsional vibration of single-walled carbon nanotube–buckyball systems. One end of the single-walled carbon nanotube (SWCNT) was fixed and the other end was used to attach the Buckyball. Civalek et al. investigated static and free torsional vibration of functionally graded (FG) nanorods using the Fourier sine series and boundary conditions were described by the two elastic torsional springs at the ends [57]. Size-dependent static and free torsional vibration responses of functionally graded porous nanotubes were examined by Uzun and Yayli by using the Fourier sine series and Stokes' transformation [43, 58]. Nazemnezhad and Fahimi studied the torsional vibration of nanobeams with a periphery crack and various end conditions [59]. Various boundary conditions, the surface shear modulus, the surface stress, and the surface density are considered on the torsional vibration of nanobeams. In another research, Nazemnezhad et al. [60] studied the effects of surface energy on the nonlinear torsional vibrations and internal resonances of nanorods. In the research, the second-order term for the angle of rotation is considered for the displacement field. They reported the conditions wherein the internal resonances occur. The effect of the surrounding elastic matrix on the axial and torsional vibrations of embedded single-walled boron nitride nanotube (SWBNNT) was studied by Uzun et al. The SWBNNT was modeled as a nanorod and the nonlocal strain gradient theory was utilized to derive the size-dependent equation of motion. Also, a one-parameter foundation model was employed to simulate the surrounding elastic matrix [61, 62]. The torsional

vibration of nanorods with torsional elastic boundary conditions via non-local elasticity theory was presented by Yayli [63].

The above literature survey shows that the linear and nonlinear torsional vibrations of nanorods in the presence of surface energy are investigated. The material properties of nanorods were assumed to be homogenous. Therefore there is a crucial question: What is the torsional behavior of nanorods in the case of functionally graded materials? It can be said that answering this question is the main goal of the present study.

2. Properties of FG Nanorod

Figure 1 shows an FG nanorod with inner radius R_i and outer radius R_o made from a graded mixture of aluminum and silicon.

The inner surface ($r = R_i$) of the FG section nanorod is a pure Al and the outer surface ($r = R_o$) is a pure Si. The properties of the FG nanorod vary through the radius direction based on power-law distribution that is stated as [60]

$$F(r) = \left(f_{r_i} - f_{r_o}\right)\left(\frac{R_o - r}{R_o - R_i}\right)^p + f_{r_o} \quad (1)$$

where $F(r) = E, \rho, G, \rho_s, \mu_s, \lambda_s$; and p is the volume fraction index which is a non-negative value.

3. Governing Equations

A nanorod with length L and diameter D is considered (Fig. 1). The cross-section of the nanorod is on the xy plane and the origin of the coordinate is set on the left side. The nanorod displacement component for torsional vibration is given as [64, 65]

$$U_x = 0 \quad (2)$$

$$U_y = -z\theta(x,t) \quad (3)$$

$$U_z = y\theta(x,t) \quad (4)$$

In the Eqs. (2)-(4), $\theta(x,t)$ is angular displacement about the center of twist, t denotes the time, and U_x, U_y, and U_z are the displacement components in the x, y, and z directions, respectively.

The geometrically nonlinear strain-displacement relationships can be represented using von-Kármán theory as follows

$$\begin{aligned}
\varepsilon_{xx} &= \frac{1}{2}(y^2 + z^2)\left(\frac{\partial\theta}{\partial x}\right)^2,\\
\varepsilon_{yy} &= \frac{1}{2}\theta^2,\\
\varepsilon_{zz} &= \frac{1}{2}\theta^2,\\
\varepsilon_{xy} &= \frac{1}{2}\left(-z\frac{\partial\theta}{\partial x} + y\theta\frac{\partial\theta}{\partial x}\right),\\
\varepsilon_{xz} &= \frac{1}{2}\left(y\frac{\partial\theta}{\partial x} + z\theta\frac{\partial\theta}{\partial x}\right),\\
\varepsilon_{yz} &= 0.
\end{aligned} \quad (5)$$

where ε is the strain. After obtaining the strains in the FG nanorod, the stress components in the bulk and the surface of the FG nanorod should be obtained.

3.1. Stress Components

The stress components (σ_{ij}) of the FG nanorod bulk are expressed based on the classical theory of elasticity as follows [66]

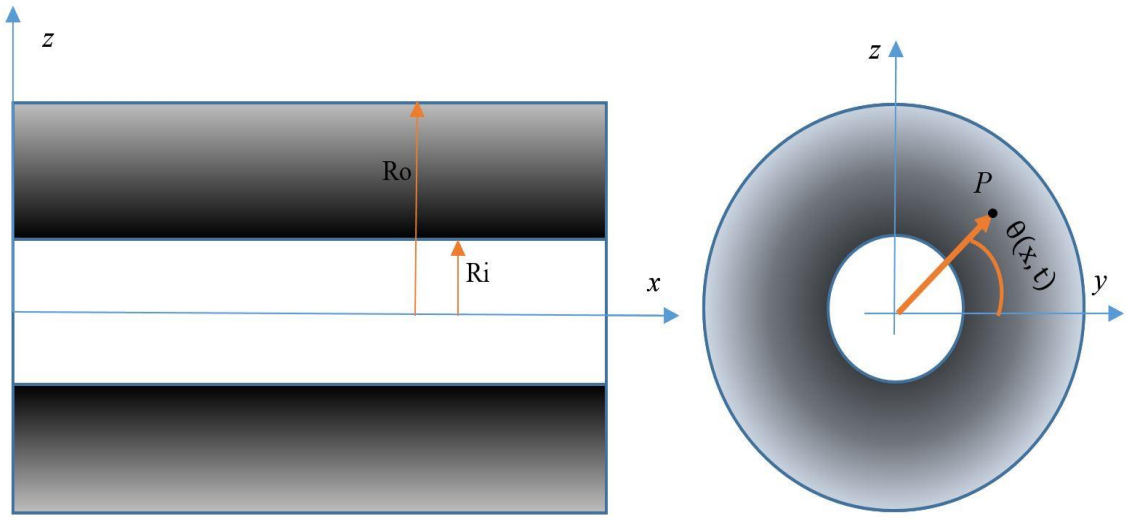

Fig. 1. Schematic of FG nanorod.

$$\sigma_{xx} = \frac{E(r)}{(1+\nu)(1-2\nu)} \times \left[\left(\frac{1-\nu}{2}\right)(y^2+z^2)\left(\frac{\partial\theta}{\partial x}\right)^2 + \nu(\theta^2)\right]$$

$$\sigma_{yy} = \frac{E(r)}{(1+\nu)(1-2\nu)} \times \left[\left(\frac{\nu}{2}\right)(y^2+z^2)\left(\frac{\partial\theta}{\partial x}\right)^2 + \left(\frac{1}{2}\right)(\theta^2)\right]$$

$$\sigma_{zz} = \frac{E(r)}{(1+\nu)(1-2\nu)} \times \left[\left(\frac{\nu}{2}\right)(y^2+z^2)\left(\frac{\partial\theta}{\partial x}\right)^2 + \left(\frac{1}{2}\right)(\theta^2)\right] \quad (6)$$

$$\sigma_{xy} = \frac{E(r)}{(1+\nu)(1-2\nu)} \times \left[\left(\frac{1-2\nu}{2}\right)\left(-z\left(\frac{\partial\theta}{\partial x}\right) + \frac{1}{2}\, y\left(\theta\frac{\partial\theta}{\partial x}\right)\right)\right]$$

$$\sigma_{xz} = \frac{E(r)}{(1+\nu)(1-2\nu)} \times \left[\left(\frac{1-2\nu}{2}\right)\left(y\left(\frac{\partial\theta}{\partial x}\right) + \frac{1}{2}\, z\left(\theta\frac{\partial\theta}{\partial x}\right)\right)\right]$$

$$\sigma_{yz} = 0.$$

To obtain the surface stress components, the Gurtin-Murdoch theory called the surface elasticity theory [66, 67] is used. The constitutive equations of the surface stresses are expressed based on the surface theory as follows

$$\sigma_{s_{ij}} = \sigma_{s_0}\,\delta_{ij} + 2(\mu_s - \sigma_{s_0})\varepsilon_{ij} + (\lambda_s + \sigma_{s\_0})U_{k,k}\delta_{ij} + \sigma_{s\_0}U_{ij} \quad (7)$$

where σ_{s_0} is the surface residual stress under unstrained conditions, λ_s and μ_s are surface Lamé constants. U_i is the displacement component of the surfaces and δ_{ij} represents the Kronecker delta.

Substituting Eqs. (2)-(4) and (5) into Eq. (7), the surface stress components (σ_{s_ij}) for the FG nanorod are obtained as

$$\begin{aligned}
&\sigma_{s_xx} = \mu_s(r)(y^2+z^2)\left(\frac{\partial\theta}{\partial x}\right)^2,\\
&\sigma_{s_yy} = \mu_s(r)\theta^2,\\
&\sigma_{s_zz} = \mu_s(r)\theta^2,\\
&\sigma_{s_xy} = 2\mu_s(r)\left[-z\frac{\partial\theta}{\partial x} + \frac{1}{2}y\theta\frac{\partial\theta}{\partial x}\right],\\
&\sigma_{s_xz} = 2\mu_s(r)\left[y\frac{\partial\theta}{\partial x} + \frac{1}{2}z\theta\frac{\partial\theta}{\partial x}\right],\\
&\sigma_{s_yz} = 0,
\end{aligned} \quad (8)$$

3.2. Governing Equations of Motion

To derive the equations of nonlinear torsional vibration of FG nanorods including the surface energy effect Hamilton's principle (Eq. (9)) is used.

$$\delta\int_{t_1}^{t_2}(U-T)dt = 0 \quad (9)$$

in Eq. (9), T and U are the kinetic and strain energies, respectively, and are given as

$$\begin{aligned}
T &= T_b + T_s\\
&= \frac{1}{2}\int_V \rho(r)\left\{\left(\frac{\partial U_y}{\partial t}\right)^2 + \left(\frac{\partial U_z}{\partial t}\right)^2\right\}dV\\
&+ \frac{1}{2}\int_A \rho_s(r)\left\{\left(\frac{\partial U_y}{\partial t}\right)^2 + \left(\frac{\partial U_z}{\partial t}\right)^2\right\}dA
\end{aligned} \quad (10)$$

$$\begin{aligned}
U &= U_b + U_s\\
&= \frac{1}{2}\int_V \{\sigma_{xx}\varepsilon_{xx} + \sigma_{yy}\varepsilon_{yy} + \sigma_{zz}\varepsilon_{zz} + \sigma_{xy}\varepsilon_{xy} + \sigma_{xz}\varepsilon_{xz}\}dV\\
&+ \frac{1}{2}\int_A \{\sigma_{s_{xx}}\varepsilon_{xx} + \sigma_{s_{yy}}\varepsilon_{yy} + \sigma_{s_{zz}}\varepsilon_{zz} + \sigma_{s_{xy}}\varepsilon_{xy} + \sigma_{s_{xz}}\varepsilon_{xz}\}dA
\end{aligned} \quad (11)$$

where ρ and ρ_s are the bulk and surface density, respectively, A is the cross-sectional area, V is the volume, T_b and T_s are the bulk and surface kinetic energies, respectively, and U_b and U_s are the bulk and surface strain energies, respectively.

Substituting Eqs. (10) and (11) into Eq. (9) and employing Hamilton's principle result in the nonlinear governing equation of motion for torsional vibration of FG nanorod and corresponding boundary condition as follows

$$\begin{aligned}
&\alpha_1\left(\frac{\partial\theta}{\partial x}\right)^2\left(\frac{\partial^2\theta}{\partial x^2}\right) + \alpha_2\theta^3 + \alpha_3\left(\frac{\partial^2\theta}{\partial x^2}\right)\\
&+\alpha_4\theta\left(\frac{\partial\theta}{\partial x}\right)^2 + \alpha_4\theta^2\left(\frac{\partial^2\theta}{\partial x^2}\right)\\
&+\alpha_5\left(\frac{\partial^2\theta}{\partial t^2}\right) = 0
\end{aligned} \quad (12)$$

$$\left(\alpha_6\left(\frac{\partial\theta}{\partial x}\right)^3 - \alpha_3\left(\frac{\partial\theta}{\partial x}\right) + \theta^3\left(\frac{\partial\theta}{\partial x}\right)\right)\delta\theta\Big|_0^l = 0 \quad (13)$$

where, α_is ($i = 1, \dots, 7$) are given as

$$\alpha_1 = -3\int_{R_i}^{R_o} 2\pi r(y^2+z^2)\mu_s(r)\,dr - \frac{3}{2}\int_{R_i}^{R_o} 2\pi r(1-\nu)(y^2+z^2)^2 A dr$$

$$\alpha_2 = 2\int_{R_i}^{R_o} 2\pi r\mu_s(r)dr + \int_{R_i}^{R_o} 2\pi r A dr$$

$$\alpha_3 = -2\int_{R_i}^{R_o} 2\pi r(y^2+z^2)^2\mu_s(r)\,dr - \frac{1}{2}\int_{R_i}^{R_o} 2\pi r(y^2+z^2)(1-2\nu)A dr$$

$$\alpha_4 = -\frac{1}{2}\int_{R_i}^{R_o} 2\pi r(y^2+z^2)^2\mu_s(r)\,dr - \int_{R_i}^{R_o} 2\pi r(y^2+z^2)\nu A dr - \frac{1}{8}\int_{R_i}^{R_o} 2\pi r(1-2\nu)(y^2+z^2)A dr \quad (14)$$

$$\alpha_5 = -\int_{R_i}^{R_o} 2\pi r(y^2+z^2)\rho(r)dr - \int_{R_i}^{R_o} 2\pi r(y^2+z^2)\rho_s(r)dr$$

$$\alpha_6 = \int_{R_i}^{R_o} 2\pi r(y^2+z^2)\mu_s(r)\,dr + \frac{1}{2}\int_{R_i}^{R_o} 2\pi r(1-\nu)(y^2+z^2)^2 A dr$$

3.3. Linear Torsional Vibration of FG Nanorods

To obtain linear mode shapes and frequencies, the nonlinear parameters in Eqs. (12) and (13) should be ignored. This results in

$$\alpha_3\frac{\partial^2\theta}{\partial x^2} + \alpha_5\frac{\partial^2\theta}{\partial t^2} = 0 \quad (15)$$

$$\left[\alpha_3\left(\frac{\partial\theta}{\partial x}\right)\right]\delta\theta\Big|_0^l = 0 \quad (16)$$

The solution of Eq. (15) can be obtained by the separation-of-variables method using the following equation

$$\theta(x,t) = \Phi(x)e^{-i\omega_L t} \quad (17)$$

where, ω_L is the natural linear torsional frequency, $\Phi(x)$ is the linear mode shape, and $i=\sqrt{-1}$ is the imaginary unit.

Substituting Eq. (17) into Eq. (15) and (16) yields the following equations

$$\alpha_3\frac{d^2\Phi}{dx^2} - \alpha_5{\omega_L}^2 = 0 \quad (18)$$

$$\left[\alpha_3\frac{d\phi}{dx}\right]\delta\Phi\Big|_0^l = 0 \quad (19)$$

Solving Eq. (18) by considering the conditions given in Eq. (19) results in the FG nanorod's mode shapes and its natural frequencies with fixed–fixed (fi-fi) and fixed–free (fi-fr) boundary conditions as below

- fi-fi end condition:

$$\Phi_n(x) = C_1 Sin\left(\frac{n\pi}{l}x\right) \quad (20)$$

$$\omega_L)_n = \left(\frac{n\pi}{l}\right)\sqrt{\frac{\alpha_3}{\alpha_5}} \quad (21)$$

- fi-free end condition:

$$\Phi_n(x) = C_1 Sin\left(\frac{(2n-1)\pi}{2l}x\right) \quad (22)$$

$$\omega_L)_n = \left(\frac{(2n-1)\pi}{l}\right)\sqrt{\frac{\alpha_3}{\alpha_5}} \quad (23)$$

3.4. Nonlinear Torsional Vibration of FG Nanorods

In the case of nonlinear torsional vibration of FG nanorod, to convert the partial differential equation (Eq. (12)) to an ordinary differential equation, the multi-mode Galerkin technique (Eq. (24)) is applied.

$$\left[\theta(x,t) = \sum_{i=1}^{N}\Phi_i(x)q_i(t)\right] \quad (24)$$

In Eq. (24), $q(t)$ denotes a time-dependent function to be determined and $\Phi(x)$ is the normalized linear mode shape function which can be obtained from Eqs. (20) and (22). Putting Eq. (24) into Eq. (12) yields

$$\left(\alpha_1\sum_{k=1}^{N}\sum_{j=1}^{N}\sum_{i=1}^{N}\frac{d\Phi_i}{dx}\frac{d\Phi_j}{dx}\frac{d^2\Phi_k}{dx^2}\right)q_iq_jq_k + \left(\alpha_2\sum_{k=1}^{N}\sum_{j=1}^{N}\sum_{i=1}^{N}\Phi_i\,\Phi_j\,\Phi_k\right)q_iq_jq_k + \left(\alpha_3\sum_{i=1}^{N}\frac{d^2\Phi_i}{dx^2}\right)q_i + \left(\alpha_4\sum_{k=1}^{N}\sum_{j=1}^{N}\sum_{i=1}^{N}\Phi_i\frac{d\Phi_j}{dx}\frac{d\Phi_k}{dx}\right)q_iq_jq_k + \left(\alpha_4\sum_{k=1}^{N}\sum_{j=1}^{N}\sum_{i=1}^{N}\Phi_i\,\Phi_j\frac{d^2\Phi_k}{dx^2}\right)q_iq_jq_k + \left(\alpha_5\sum_{i=1}^{N}\Phi_i\right)\ddot{q}_\iota = 0 \quad (25)$$

In the next step, the following dimensionless parameters are defined

$$X=\frac{x}{L}\ ;\ \bar{q}=\frac{q}{q_{max}};\ \bar{\Phi}=\frac{\Phi}{L} \quad (26)$$

where q_{max} denotes the maximum amplitude of the time-dependent function $q(t)$.

Using the dimensionless parameters in Eq. (25), multiplying Eq. (25) by the normalized linear mode shape $\Phi(X)$, and integrating from X = 0 to X = 1, results in the following equation

$$\left\{\frac{\alpha_1}{\alpha_5L^2}\sum_{k=1}^{n}\sum_{j=1}^{n}\sum_{i=1}^{n}(\beta_1)_{mijk} + \frac{\alpha_2L^2}{\alpha_5}\sum_{k=1}^{n}\sum_{j=1}^{n}\sum_{i=1}^{n}(\beta_2)_{mijk} + \frac{\alpha_4}{\alpha_5}\sum_{k=1}^{n}\sum_{j=1}^{n}\sum_{i=1}^{n}(\beta_3)_{mijk} + \frac{\alpha_4}{\alpha_5}\sum_{k=1}^{n}\sum_{j=1}^{n}\sum_{i=1}^{n}(\beta_4)_{mijk}\right\}{q_{max}}^2\bar{q}_\iota\bar{q}_j\bar{q}_k + {\omega_m}^2\bar{q}_m + \ddot{\bar{q}}_m = 0 \quad (27)$$

in which the parameters $(\beta_1)_{mijk}$, $(\beta_2)_{mijk}$, $(\beta_3)_{mijk}$ and $(\beta_4)_{mijk}$ are specified as:

$$(\beta_1)_{mijk}=\int_0^1\left(\Phi_m\frac{d\Phi_i}{dX}\frac{d\Phi_j}{dX}\frac{d^2\Phi_k}{dX^2}\right)dX$$
$$(\beta_2)_{mijk}=\int_0^1\left(\Phi_m\Phi_i\Phi_j\Phi_k\right)dX$$
$$(\beta_3)_{mijk}=\int_0^1\left(\Phi_m\Phi_i\frac{d\Phi_j}{dX}\frac{d\Phi_k}{dX}\right)dX \quad (28)$$
$$(\beta_4)_{mijk}=\int_0^1\left(\Phi_m\Phi_i\Phi_j\frac{d^2\Phi_k}{dX^2}\right)dX$$

and the following relations are used

$$\begin{cases}\int_0^1\overline{\Phi_m}(x)\bar{\Phi}_\iota(x)dX=\delta_{im}\\ \int_0^1\overline{\Phi_m}(x)\dfrac{d^2\bar{\Phi}_\iota(x)}{dX^2}dX=-\lambda_m^2\delta_{im}\\ \omega_m^2=-\dfrac{\alpha_3{\lambda_m}^2}{\alpha_5L^2}\end{cases} \quad (29)$$

where in Eqs. (28) and (29) λ_m and $\bar{\Phi}_m(X)$ are defined as

- $\lambda_m=m\pi$;

$$\bar{\Phi}_m=\sqrt{2}Sin(\lambda_mX) \quad (30)$$

(fi-fi end conditions)

- $\lambda_m=(2m-1)\frac{\pi}{2}$;

$$\bar{\Phi}_m=\sqrt{2}Sin(\lambda_mX) \quad (31)$$

(fi-free end conditions)

4. Solution Method

The multiple scale method is employed to solve the nonlinear equation, Eq. (27). To this end, the small dimensionless parameter ε is introduced. Therefore, Eq. (27) can be rewritten as follows

$$\ddot{\bar{q}}_m+{\omega_m}^2\bar{q}_m + \varepsilon\left\{\frac{\alpha_1}{\alpha_5L^2}\sum_{k=1}^{n}\sum_{j=1}^{n}\sum_{i=1}^{n}(\beta_1)_{mijk} + \frac{\alpha_2L^2}{\alpha_5}\sum_{k=1}^{n}\sum_{j=1}^{n}\sum_{i=1}^{n}(\beta_2)_{mijk} + \frac{\alpha_4}{\alpha_5}\sum_{k=1}^{n}\sum_{j=1}^{n}\sum_{i=1}^{n}(\beta_3)_{mijk} + \frac{\alpha_4}{\alpha_5}\sum_{k=1}^{n}\sum_{j=1}^{n}\sum_{i=1}^{n}(\beta_4)_{mijk}\right\}{q_{max}}^2\bar{q}_\iota\bar{q}_j\bar{q}_k = 0 \quad (32)$$

To use the method of multiple scales, the solution of Eq. (32) can be represented by an expansion having the following form

$$\bar{q}_m(t_i;\varepsilon)=\bar{q}_{m_0}(t_0,t_1)+\varepsilon\bar{q}_{m_1}(t_0,t_1)+\varepsilon^2\bar{q}_{m_2}(t_0,t_1)+\cdots \quad (33)$$

in Eq. (33), $t_0 = t$ denotes time scale that shows oscillatory effect and $t_n=\varepsilon^nt$.

Substituting Eq. (33) into Eq. (32) and setting the coefficients with a similar power equal to zero leads to the following set of differential equations:

$$\varepsilon^0: \quad {D_0}^2\bar{q}_{m_0} + {\omega_m}^2\bar{q}_{m_0} = 0 \tag{34}$$

$$\varepsilon^1: \quad {D_0}^2\bar{q}_{m1} + {\omega_m}^2\bar{q}_{m1} = -2D_0D_1\bar{q}_{m0} + (\beta)_{mmmm}{q_{max}}^2{\bar{q}_{m_0}}^3 \tag{35}$$

$$\begin{aligned}\varepsilon^2: \quad & {D_0}^2\bar{q}_{m2} + {\omega_m}^2\bar{q}_{m2} = -\left({D_1}^2 + 2D_0D_1\right)\bar{q}_{m0} - 2D_0D_1\bar{q}_{m1} - \\ & -{q_{max}}^2{\bar{q}_{m0}}^2\left\{\sum_{j=1}^{n}\bar{q}_{j1}\left(\left(\frac{\alpha_1}{\alpha_5 l^2}\left((\beta_1)_{mjmm} + (\beta_1)_{mmjm} + (\beta_1)_{mmmj}\right)\right) + \left(\frac{\alpha_2 l^2}{\alpha_5}\left((\beta_2)_{mjmm} + \right.\right.\right.\right. \\ & \left.(\beta_2)_{mmjm} + (\beta_2)_{mmmj}\right)\Big) + \left(\frac{\alpha_4}{\alpha_5}\left((\beta_3)_{mjmm} + (\beta_4)_{mjmm} + (\beta_3)_{mmjm} + (\beta_4)_{mmjm} + \right.\right. \\ & \left.\left.\left.\left.(\beta_3)_{mmmj} + (\beta_4)_{mmmj}\right)\right)\right)\right\}\end{aligned} \tag{36}$$

where

$$(\beta)_{mmmm} = \left(\frac{\alpha_1}{\alpha_5 l^2}(\beta_1)_{mmmm} + \frac{\alpha_2 l^2}{\alpha_5}(\beta_2)_{mmmm} + \frac{\alpha_4}{\alpha_5}\left((\beta_3)_{mmmm} + (\beta_4)_{mmmm}\right)\right) \text{ and } D_i = \frac{\partial}{\partial t_i}.$$

A general solution for Eq. (34) can be given as

$$\begin{aligned}&\bar{q}_{m_0} = A_m e^{i\omega_m t_0} + \bar{A}_m\, e^{-i\omega_m t_0},\\ &\bar{q}_{n_0} = 0 \quad for \quad n \neq m.\end{aligned} \tag{37}$$

A_m and $\bar{A}_m$ are a complex function and the complex conjugate of A_m, respectively; These functions can be determined by eliminating the secular terms from $\bar{q}_1$. For this purpose, $\bar{q}_{m_0}$ and $\bar{q}_{n_0}$ from Eq. (37) should be substituted into Eq. (35).

This results in

$$\begin{aligned}&{D_0}^2\bar{q}_{m_1} + {\omega_m}^2\bar{q}_{m_1} = \\ &-(D_1A_m)(2i\omega_m e^{i\omega_m t_0}) \\ &+{q_{max}}^2\left(\frac{\alpha_1}{\alpha_5 L^2}\left((\beta_1)_{mmmm}{A_m}^3 e^{3i\omega_m t_0}\right.\right. \\ &+ 3(\beta_1)_{mmmm}{A_m}^2\bar{A}_m e^{i\omega_m t_0}\Big) \\ &+ \frac{\alpha_2 L^2}{\alpha_5}\left((\beta_2)_{mmmm}{A_m}^3 e^{3i\omega_m t_0}\right. \\ &+ 3(\beta_2)_{mmmm}{A_m}^2\bar{A}_m e^{i\omega_m t_0}\Big) \\ &+ \frac{\alpha_4}{\alpha_5}\Big(\left((\beta_3)_{mmmm}\right. \\ &+ (\beta_4)_{mmmm})A_m{}^3 e^{3i\omega_m t_0} \\ &+ 3((\beta_3)_{mmmm} \\ &\left.\left.+ (\beta_4)_{mmmm}){A_m}^2\bar{A}_m e^{i\omega_m t_0}\Big)\right) + CC\end{aligned} \tag{38}$$

$$\begin{aligned}&{D_0}^2\bar{q}_{n_1} + {\omega_m}^2\bar{q}_{n_1} \\ &= {q_{max}}^2\left(\frac{\alpha_1}{\alpha_5 L^2}\left((\beta_1)_{mmmm}{A_m}^3 e^{3i\omega_m t_0}\right.\right. \\ &+ 3(\beta_1)_{mmmm}{A_m}^2\bar{A}_m e^{i\omega_m t_0}\Big) \\ &+ \frac{\alpha_2 L^2}{\alpha_5}\left((\beta_2)_{mmmm}{A_m}^3 e^{3i\omega_m t_0}\right. \\ &+ 3(\beta_2)_{mmmm}{A_m}^2\bar{A}_m e^{i\omega_m t_0}\Big) \\ &+ \frac{\alpha_4}{\alpha_5}\Big(\left((\beta_3)_{mmmm}\right. \\ &+ (\beta_4)_{mmmm})A_m{}^3 e^{3i\omega_m t_0} \\ &+ 3((\beta_3)_{mmmm} \\ &\left.\left.+ (\beta_4)_{mmmm}){A_m}^2\bar{A}_m e^{i\omega_m t_0}\Big)\right) + CC\end{aligned} \tag{39}$$

In Eq. (39) CC denotes the complex conjugate of the past terms. The resonance effect in these equations must be eliminated, so we do

$$\begin{aligned}&-D_1A_m(2i\omega_m e^{i\omega_m t_0}) \\ &+3{q_{max}}^2\left\{(\beta)_{mmmm}{A_m}^2\bar{A}_m e^{i\omega_m t_0}\right\} = 0\end{aligned} \tag{40}$$

Now, the solution of Eqs. (38) and (39) are expressed as

$$\begin{aligned}&\bar{q}_{m_1} = \\ &\quad -\frac{{q_{max}}^2}{8{\omega_m}^2}((\beta)_{mmmm}){A_m}^3 e^{3i\omega_m t_0} + CC\end{aligned} \tag{41}$$

$$\begin{aligned}&\bar{q}_{n_1} = \\ &\quad \frac{3{q_{max}}^2}{({\omega_n}^2 - {\omega_m}^2)}((\beta)_{mmmm}){A_m}^2\overline{A_m}e^{i\omega_m t_0} \\ &\quad + \frac{{q_{max}}^2}{({\omega_n}^2 - 9{\omega_m}^2)}((\beta)_{mmmm}){A_m}^3 e^{3i\omega_m t_0} \\ &\quad + CC\end{aligned} \tag{42}$$

To solve Eq. (40), $A_m$is expressed in the polar form

$$A_m = \frac{1}{2} a_m e^{ib_m} \tag{43}$$

where a and b are real parameters.

Substituting Eq. (43) into Eq. (40) and separating the real and imaginary sections equal to zero, leads to the following equations

$$\begin{aligned} &\boldsymbol{Im}: \omega_m (D_1 a_m) = 0 \xrightarrow{yields} \\ &a_m = constant \\ &\boldsymbol{Re}: -a_m \omega_m (D_1 b_m) + \frac{3{q_{max}}^2 {a_m}^3}{8} (\beta)_{mmmm} = 0 \xrightarrow{yields} \\ &b_m = \frac{3{q_{max}}^2 {a_m}^2}{8\omega_m} (\beta)_{mmmm} t_1 + b_{m0} \end{aligned} \tag{44}$$

where b_{m0} is a constant. Putting the results of Eqs. (44) into Eq. (43), A_m is obtained as

$$\begin{aligned} &A_m \\ &= \frac{1}{2} a_m e^{i\left(\frac{3{q_{max}}^2 {a_m}^2}{8\omega_m} (\beta)_{mmmm} t_1 + b_{m0}\right)} \\ &= \frac{1}{2} a_m e^{i\left(\frac{3{q_{max}}^2 {a_m}^2}{8\omega_m} (\beta)_{mmmm} \varepsilon t + b_{m0}\right)} \end{aligned} \tag{45}$$

Substituting Eqs. (45), (42), (41), and (37) into Eq. (33) results in [69]

$$\begin{aligned} &\bar{q}_m \\ &= A_m e^{i\omega_m t_0} \\ &+ \varepsilon \left(-\frac{{q_{max}}^2}{8{\omega_m}^2} ((\beta)_{mmmm} {A_m}^3 e^{3i\omega_m t_0} \right) \\ &+ CC \end{aligned} \tag{46}$$

$$\begin{aligned} &\bar{q}_n \\ &= \varepsilon \left(\frac{3{q_{max}}^2}{({\omega_n}^2 - {\omega_m}^2)} ((\beta)_{mmmm} {A_m}^2 \overline{A_m} e^{i\omega_m t_0} \right. \\ &\left. + \frac{{q_{max}}^2}{({\omega_n}^2 - 9{\omega_m}^2)} ((\beta)_{mmmm} {A_m}^3 e^{3i\omega_m t_0} \right) \\ &+ CC \end{aligned} \tag{47}$$

Eqs. (46) and (47) can be rewritten as

$$\begin{aligned} &\bar{q}_m = a_m \cos(\theta) \\ &+ \varepsilon \left[-\frac{{q_{max}}^2}{32{\omega_m}^2} {a_m}^3 (\beta)_{mmmm} \right] \cos(3\theta) + O(\varepsilon^2) \end{aligned} \tag{48}$$

$$\begin{aligned} &\bar{q}_n = \varepsilon \left(\left(\frac{3{q_{max}}^2}{4({\omega_n}^2 - {\omega_m}^2)} {a_m}^3 (\beta)_{mmmm} \right) \cos(\theta) + \right. \\ &\left. \left(\frac{{q_{max}}^2}{4({\omega_n}^2 - 9{\omega_m}^2)} {a_m}^3 (\beta)_{mmmm} \right) \cos(3\theta) \right) + O(\varepsilon^2) \end{aligned} \tag{49}$$

where

$$\begin{aligned} &\theta = \omega_m^{nl} t + b_{m0} \\ &\omega_m^{nl} = \omega_m + \varepsilon \frac{3{q_{max}}^2 {a_m}^2}{8\omega_m} (\beta)_{mmmm} \end{aligned} \tag{50}$$

ω_m^{nl} denotes the nonlinear and ω_m is the linear natural frequency. Since ε represents a bookkeeping device, we put it equal to unity and for satisfying the initial conditions ($\bar{q}_m(0) = 0, \dot{\bar{q}}_m(0) = 0$) in Eq. (44), the error related to the second-order expansion should be taken into account. These yields $b_{m0} = 0, a_m = 1$.

Eq. (49) displays that internal resonances occur in two cases, one-to-one ($\omega_n = \omega_m$), and three-to-one ($\omega_n = 3\omega_m$).

5. Numerical Results

Before the presentation of graphical and numerical results, a comparative study is conducted to verify the applicability and accuracy of the present formulation. Due to the lack of a similar problem and solution, the accuracy of the present solution is verified by comparing the results with those of Setoodeh et al. [66]. The Young's modulus and density of the nanorod were taken as 70 GPa and 2700 kg/m^3, respectively while the Poisson's ratio (ϑ) is 0.23. In Table 1 natural frequencies of FGM nanorods are listed for various vibration amplitudes, mode numbers, and nanorod lengths. As shown in Table 1, the reliability of the present formulation and results is confirmed. However, a slight difference between reported frequencies can be observed, which is attributed to different methods of solution. In the current study, the technique of multiple scales has been used to characterize the dynamic characteristics of the nanorod, while Setoodeh et al. [66] used the Homotopy Analysis Method to identify linear and nonlinear torsional free vibration of functionally graded micro/nano-tubes.

In the following, the linear and nonlinear frequencies of nanorods are presented by considering the surface effects, the frequency number, the amplitude of nonlinear vibrations, and the radius and the length of the nanorod. In Table 2, the bulk and the surface elastic properties of aluminum (Al) and silicon (Si) are presented. The crystallographic directions of aluminum and silicon are [1 1 1] and [1 0 0], respectively.

The ratio of frequency is calculated as follows to demonstrate how surface components affect the natural torsional frequencies of nanorods:

$$FR = \frac{f_s}{f_c} \tag{51}$$

in which f_s is the natural torsional frequency of nanorods with surface energy effects and f_c is the natural torsional frequency of nanorods without surface energy effects. It can be seen from this equation if the frequency ratio is less than one, then the surface parts have a decremental effect and vice versa. Furthermore, as the frequency

ratio is one, the natural torsional frequency is not affected by the surface components.

Firstly, the effect of surface energy parameters on the torsional vibration of FG nanorods is investigated in Table 3. Listed in Table 3 are linear and nonlinear torsional frequencies of FG nanorod for various amplitudes of vibration, nanorod radii, mode numbers, and end conditions, i.e. fi-fi and fi-fr. Based on this table, the following results can be obtained. In both linear and nonlinear vibrations surface density has a decreasing effect on the natural frequencies of the nanorod. This reduction effect is independent of the amplitude of vibrations, mode number, and type of boundary condition but it depends on the radius of the nanotube and the FG power index. It is seen from Table 3, that as the FG power index grows, the reducing effect of the surface density parameter rises. This is due to the increase in the amount of surface density with increasing the FG power index and since increasing the density increases the kinetic energy, the frequency decreases. Another result obtained from Table 3 is the reduction in the reducing effect of surface density by growing the radius of the nanorod. As another result of Table 3, it can be mentioned the effect of increasing the radius of the nanorod in reducing the effect of surface density.

Table 1. Comparison of nonlinear torsional frequencies (GHz) for various lengths and mode numbers (all surface parameters considered to be zero).

Amplitude of vibration	Length (nm)	Mode number	Setoodeh et al. [68]	Present study
0.001	10	1st	167.422	167.409
		2nd	363.744	363.430
	15	1st	109.738	109.736
		2nd	228.380	228.331
0.010	10	1st	441.133	434.047
		2nd	1672.54	1639.00
	15	1st	212.00	209.533
		2nd	760.65	746.79

Table 2. Bulk and the surface elastic properties of aluminum and silicon

Material	Bulk elastic properties		Surface elastic properties	
	$G(Gpa)$	$\rho(kg/m^3)$	$\bar{\rho}(kg/m^2)$	$\bar{\mu}(N/m)$
Al (internal surface)	28.5	2700	$10^{-7}\times5.46$	-0.8269
Si (external surface)	86	1250	$10^{-7}\times3.17$	-2.7779

Table 3. Linear and nonlinear torsional frequency ratios of FG nanorod

Boundary condition	R_o (nm)	n	q_{max}	Only ρ_s			Only μ_s			Both ρ_s, μ_s		
				p			p			p		
				0	1	100	0	1	100	0	1	100
Fixed-Fixed	1	1	0.00	0.8882	0.8879	0.8676	0.9621	0.9551	0.9560	0.8545	0.8481	0.8294
			0.05	0.8882	0.8879	0.8676	0.9743	0.9740	0.9733	0.8653	0.8648	0.8445
			0.10	0.8882	0.8879	0.8676	0.9896	0.9937	0.9933	0.8789	0.8824	0.8618
		5	0.00	0.8882	0.8879	0.8676	0.9621	0.9551	0.9560	0.8545	0.8481	0.8294
			0.05	0.8882	0.8879	0.8676	0.9629	0.9563	0.9571	0.8552	0.8491	0.8304
			0.10	0.8882	0.8879	0.8676	0.9650	0.9597	0.9601	0.8571	0.8521	0.8330
	2	1	0.00	0.9388	0.9386	0.9263	0.9805	0.9776	0.9780	0.9205	0.9176	0.9059
			0.05	0.9388	0.9386	0.9263	0.9828	0.9806	0.9807	0.9227	0.9204	0.9085
			0.10	0.9388	0.9386	0.9263	0.9877	0.9867	0.9865	0.9272	0.9262	0.9138
		5	0.00	0.9388	0.9386	0.9263	0.9805	0.9776	0.9780	0.9205	0.9176	0.9059
			0.05	0.9388	0.9386	0.9263	0.9808	0.9779	0.9782	0.9207	0.9178	0.9062
			0.10	0.9388	0.9386	0.9263	0.9814	0.9786	0.9790	0.9213	0.9185	0.9068
Fixed-Free	1	1	0.00	0.8882	0.8879	0.8676	0.9621	0.9551	0.9560	0.8545	0.8481	0.8294
			0.05	0.8882	0.8879	0.8676	0.9895	0.9937	0.9933	0.8789	0.8823	0.8618
			0.10	0.8882	0.8879	0.8676	1.0021	1.0073	1.0084	0.8900	0.8945	0.8749
		5	0.00	0.8882	0.8879	0.8676	0.9621	0.9551	0.9560	0.8545	0.8481	0.8294
			0.05	0.8882	0.8879	0.8676	0.9630	0.9566	0.9573	0.8553	0.8494	0.8305
			0.10	0.8882	0.8879	0.8676	0.9655	0.9605	0.9608	0.8575	0.8529	0.8336
	2	1	0.00	0.9388	0.9386	0.9263	0.9805	0.9776	0.9780	0.9205	0.9176	0.9059
			0.05	0.9388	0.9386	0.9263	0.9876	0.9867	0.9864	0.9272	0.9261	0.9137
			0.10	0.9388	0.9386	0.9263	0.9957	0.9958	0.9959	0.9348	0.9347	0.9225
		5	0.00	0.9388	0.9386	0.9263	0.9805	0.9776	0.9780	0.9205	0.9176	0.9059
			0.05	0.9388	0.9386	0.9263	0.9808	0.9779	0.9783	0.9207	0.9178	0.9062
			0.10	0.9388	0.9386	0.9263	0.9814	0.9787	0.9790	0.9213	0.9186	0.9069

As the radius of the nanorod increases, the energy stored in its volume and surface increases, but the rate of the energy stored in the volume of the nanorod is more than the energy stored on its surface. Therefore, the ratio of the total volume energy to the surface energy will be greater than before. As a result, the effect of surface density becomes less.

According to Table 3, it can be seen that the effect of the Lamé constant on the natural frequency of nanorod is a little different from the effect of the surface density parameter. It is readily apparent from Table 3 that in the case of linear vibrations, the surface Lamé constant has a decreasing effect on the torsional frequencies of the FG nanorod. This decreasing effect is independent of the frequency mode number and boundary end conditions but depends on the value of the power index and the nanorod radius. There is no determined relationship between the reducing effect of the Lamé constant on the natural frequency and the value of the FG power index. As the value of the FG index increases from 0 to 1, the reducing effect of the Lamé constant rises. Then, by growing m from 1 to 100, the decreasing effect of the Lamé constant on the natural frequency reduces. In the end, the reduction effect of the Lamé constant on the natural frequency of nanorod for m = 0 (i.e. Al nanorod) is less than for m = 100 (i.e. Si nanorod). The reason for this is the difference in the amount of Al and Si Lamé constant. Because the dependence of the Lamé constant reduction effect on the FG nanorod radius has a reason similar to the dependence of the surface density reducing effect on the FG nanorod radius, its repetition is avoided.

In general, it can be said that the Lamé constant has a reducing influence on the torsional frequencies of the FG nanorod in the case of nonlinear vibrations. This decreasing effect depends not only on the frequency number and the boundary conditions but also depends on the amplitude of the nonlinear vibrations and the radius of the FG nanorod. However, according to Table 3, for the high amplitude of vibrations and the C-F boundary condition, the Lamé constant has an increasing effect. The dependence of the Lamé constant effect on the value of the FG index is similar to that of linear vibrations. Based on Table 3, by increasing the amplitude of nonlinear vibrations and assuming that other parameters do not change, the decreasing effect of the Lamé constant reduces. Because with increasing amplitude of vibrations, the strain energy in the volume of nanorods increases at a higher rate than the strain energy at the surface of the nanorod. The rate of this growth is higher in the higher frequencies number and for the fi-fi boundary condition. Another result shown in Table 3 is that like linear vibrations, the decreasing effect of the Lame constant decreases with the increasing radius of the FG nanorod. Finally, it can be seen from Table 3 that the reduction effect of the Lamé constant on the torsional frequencies of the FG nanorod is higher for nanorods with fi-fr end conditions than for nanorods with fi-fi end conditions.

Finally, the decreasing effects of surface density and surface Lamé constant on the linear and nonlinear torsional frequencies of the FG nanotube become apparent as a cumulative effect when both variables are considered. Table 3 displays that the reducing effect of the effective surface parameters on the torsional vibration behavior of the FG nanorods, in the case of linear vibrations, is independent of the boundary condition and frequency number. However, in the case of nonlinear vibrations, the mentioned reduction effect depends on all factors, including the type of boundary condition, the radius of the nanorod, the amplitude of the vibrations, and the frequency number. The manner of dependence and the type of effect on the nonlinear torsional frequencies of the FG nanotubes are similar to those stated for the case only considering the effect of the Lamé surface constant, and its explanations are omitted to avoid repetition.

The variation of the torsional frequency of the FG nanorod against the nanorod length for various FG power indexes, mode numbers, vibration amplitude, and type of boundary conditions is presented in Figs. 2a-2h. It can be found that for shorter nanorods and by increasing the FG power index, the decreasing effect of surface parameters reduces. The reason for the greater decreasing effect of surface parameters on the torsional frequencies of nanorods with shorter lengths is that the shorter the nanorod length, the greater the ratio of energy stored at the surface to energy stored at volume.

In addition, it is also observed that as the length of the FG nanorod increases, both the frequency and the decreasing effect of the surface parameters lessen. This behavior is observed for different values of the FG power index, vibration amplitude, type of boundary condition, and frequency number.

The conditions for occurring internal resonances of C-C and C-F nanorods with and without the effect of surface parameters are listed in Tables 4a and 4b. It is clear that considering the surface parameters changes the internal resonance ratio, and its value depends on the type of boundary condition. Another point that can be seen from Tables 4a and 4b is that considering the surface parameters and for

certain values of m, n, and q_{max}, internal resonances occur for different values of the FG power index at different nanometer lengths. For a given value of *m*, *n*, and *p* by increasing the amplitude of the vibrations, the internal resonances of the nanorod occur in shorter lengths. On the contrary, for certain values of p, n, and q_{max} as the frequency number increases, the internal resonance of the FG nanorod occurs at longer lengths.

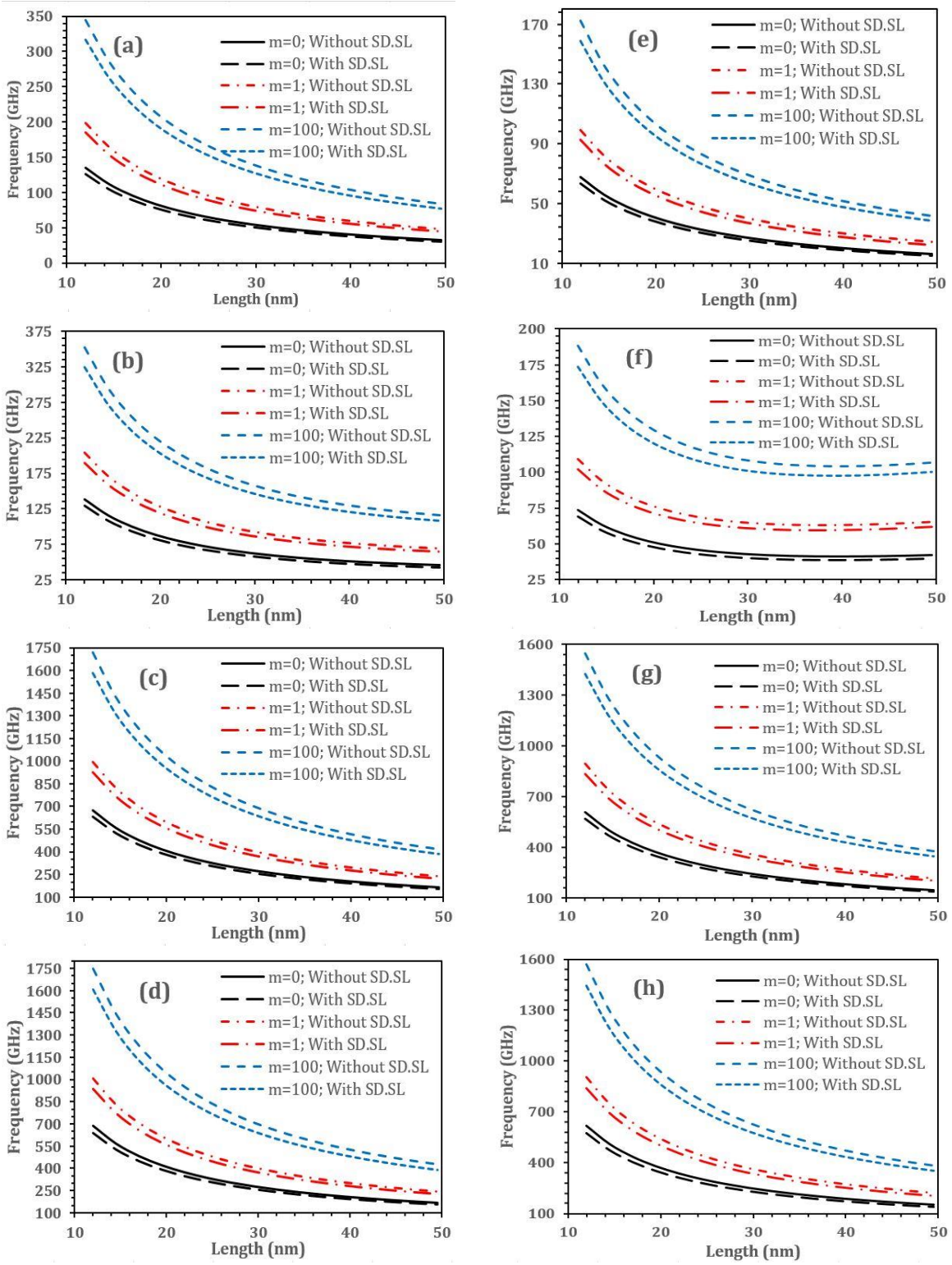

Fig. 2. Variations of axial frequencies versus the nanorod length, Ro=2.25 nm, Ri=1.25, a) Fi-Fi, n=1, qmax=0; b) Fi-Fi, n=1, qmax=0.05; c) Fi-Fi, n=5, qmax=0; d) Fi-Fi, n=5, qmax=0.05; e) Fi-Fr, n=1, qmax=0; f) Fi-Fr, n=1, qmax=0.05; g) Fi-Fr, n=5, qmax=0; h) Fi-Fr, n=5, qmax=0.05 (SD.SL means surface density and surface Lamé constants).

Table 4a. Various conditions for occurring internal resonances of fixed-fixed FG nanorod with and without surface effects (R_o=1.5 nm and R_i=0.25 nm).

n	m	q_{max}	p	Length (nm)	ω_n/ω_m	
					Without surface effect	With surface effect
4	1	0.07	0	20.26	3.0000	2.9754
			1	18.57	3.0000	2.9721
			100	20.16	3.0000	2.9715
4	1	0.08	0	17.79	3.0000	2.9748
			1	16.31	3.0000	2.9718
			100	17.70	3.0000	2.9714
4	1	0.09	0	15.88	3.0000	2.9754
			1	14.56	3.0000	2.9729
			100	15.80	3.0000	2.9721
4	1	0.10	0	14.38	3.0000	2.9755
			1	13.19	3.0000	2.9730
			100	14.31	3.0000	2.9718
5	1	0.07	0	28.34	3.0000	2.9602
			1	25.97	3.0000	2.9556
			100	28.20	3.0000	2.9546
5	1	0.08	0	24.85	3.0000	2.9596
			1	22.77	3.0000	2.9556
			100	24.72	3.0000	2.8123
5	1	0.09	0	22.14	3.0000	2.9603
			1	20.29	3.0000	2.9563
			100	22.03	3.0000	2.9548
5	1	0.10	0	19.99	3.0000	2.9610
			1	18.33	3.0000	2.9562
			100	19.89	3.0000	2.9556

Table 4b. Various conditions for occurring internal resonances of fixed-free FG nanorod with and without surface effects (R_o=1.5 nm and R_i=0.25 nm).

n	m	q_{max}	p	Length (nm)	ω_n/ω_m	
					Without surface effect	With surface effect
4	1	0.07	0	19.83	3.0000	2.9427
			1	18.17	3.0000	2.9364
			100	19.72	3.0000	2.9369
4	1	0.08	0	17.37	3.0000	2.9439
			1	15.92	3.0000	2.9370
			100	17.28	3.0000	2.9369
4	1	0.09	0	15.47	3.0000	2.9440
			1	14.18	3.0000	2.9373
			100	15.39	3.0000	2.9370
4	1	0.10	0	13.96	3.0000	2.9439
			1	12.79	3.0000	2.9394
			100	13.89	3.0000	2.9364
5	1	0.07	0	24.15	3.0000	2.9334
			1	22.13	3.0000	2.9257
			100	24.02	3.0000	2.9260
5	1	0.08	0	21.26	3.0000	2.9153
			1	19.39	3.0000	2.9263
			100	21.05	3.0000	2.9255
5	1	0.09	0	18.84	3.0000	2.9346
			1	17.27	3.0000	2.9277
			100	18.74	3.0000	2.9269
5	1	0.10	0	17.00	3.0000	2.9344
			1	15.58	3.0000	2.9279
			100	16.91	3.0000	2.9267

The variations of the natural frequencies versus vibration amplitude for various cases are presented in Figs. 3a-3d. In these figures, the first and fifth modes of FG nanorods with fi-fi and fi-fr boundary conditions are considered. It is observed that for both boundary conditions, overall variations of frequencies are the same and this trend can be observed in different mode numbers. In addition, it is revealed that as the amplitude of vibrations increases, the natural frequency of FG nanorod rises and the magnitude of the increase is greater at higher amplitudes. These changes are more obvious at lower mode numbers. The other results are the same as those reported before, therefore they are not repeated here again.

In the end, the effect of radius variations on the natural frequency of FG nanorod is investigated in Figs. 4a-4h. By comparing the curves in linear and nonlinear vibration modes, it is observed that the effect of surface energy on linear and nonlinear frequencies is different from each other (as explained before in Table 3). Also, depending on the different mode numbers, the effect of surface energy on the natural frequencies of FG nanorod is various. In Figs 4a-4h, the effect of surface energy on the natural frequencies of the nanorod can be seen for different values of the FG power index and different radii of the nanorod (as seen before in Table 3).

6. Conclusions

In this study, nonlinear torsional vibrations of functionally graded nanorods are investigated using surface elasticity theory and the conditions for which internal resonances occur. Recently, FGMs have been used in micro/nano-structures and atomic force microscopes (AFMs). It is necessary to enhance the knowledge about the mechanical response of the FGMs for the next technological revolution since these structures are emerging as the new generation of micro/nano-tubes offering exciting physical and mechanical properties. The main conclusions are as follows:

1. Surface parameters have a reducing effect on the torsional frequencies of functionally graded nanorods.
2. Linear and nonlinear frequencies of functionally graded nanorods with shorter lengths are more sensitive to surface parameters for larger power index values.
3. By increasing the amplitude of nonlinear vibrations, the frequencies of functionally graded nanorods are less affected by the surface parameters and the amount of this influence depends on the power index.

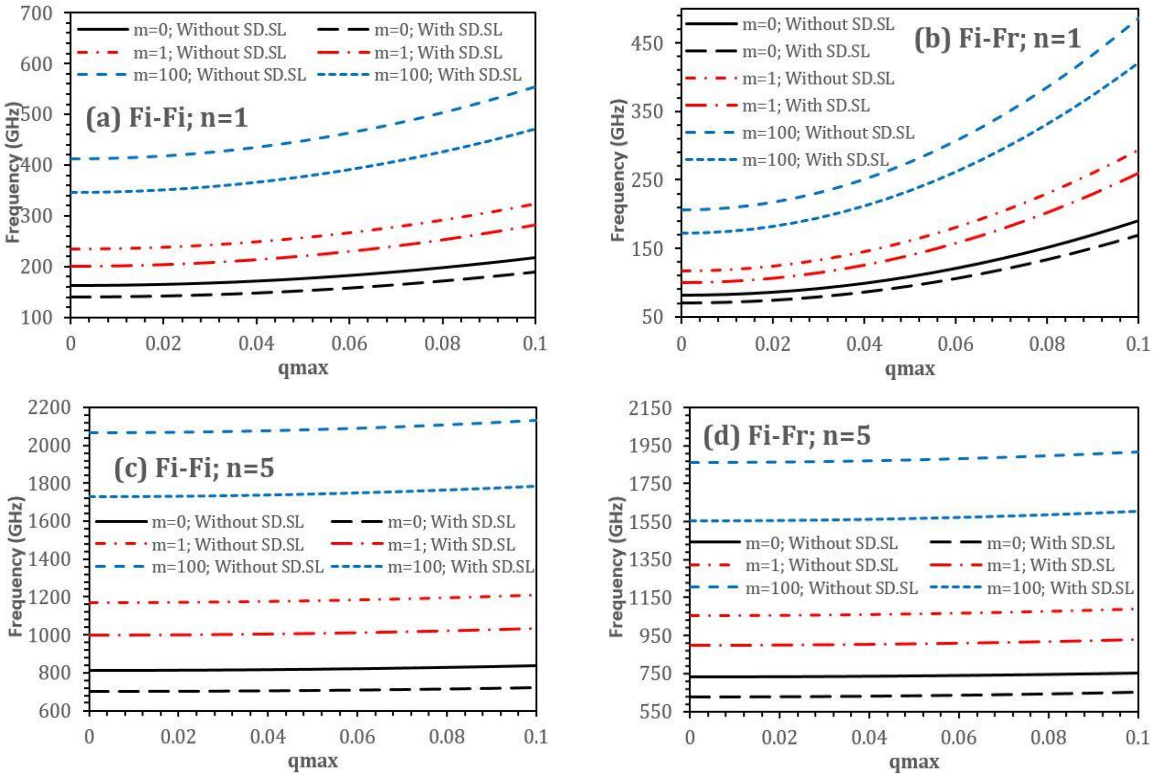

Fig. 3. Variations of axial frequencies versus the amplitude of vibration, (L=10 nm, Ro=1 nm, Ri=0.5 nm; and SD.SL means surface density and surface Lamé constants.)

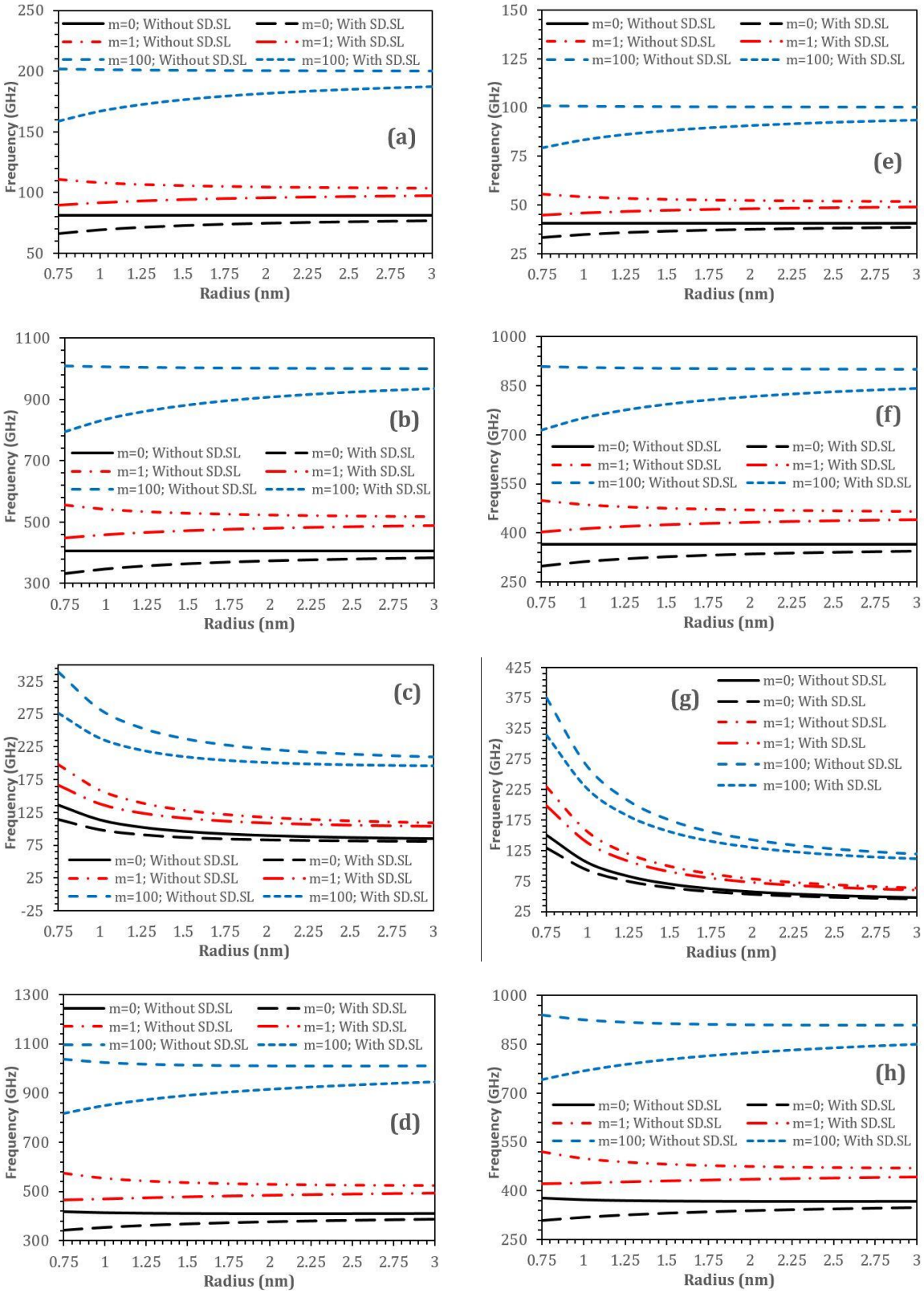

Fig. 4. Variations of frequency versus the nanorod radius (R_i=0.25 nm, L=20 nm), a) fixed-fixed, n=1, q_{max}=0; b) fixed-fixed, n=5, q_{max}=0; c) fixed-fixed, n=1, q_{max}=0.05; d) fixed-fixed, n=5, q_{max}=0.05; e) fixed-free, n=1, q_{max}=0; f) fixed-free, n=5, q_{max}=0; g) fixed-free, n=1, q_{max}=0.05; h) fixed-free, n=5, q_{max}=0.05 (SD.SL means surface density and surface Lamé constants).

4. Depending on the value of the power index, the influence of the surface parameters on the torsional frequencies of functionally graded nanorods is different for various values of nanorod radius, frequency number, and types of boundary conditions.
5. Considering the surface parameters changes the conditions of the internal resonances of the FG nanorod. This change is such that the higher the value of the power index, the deviation of the internal resonance ratio considering the surface parameters is greater than the internal resonance ratio of the classical state (without considering the surface parameters).

Conflicts of Interest

The author declares that there is no conflict of interest regarding the publication of this manuscript.

Reference

[1] Abdelaziz, H.H., Meziane, M.A.A., Bousahla, A.A., Tounsi, A., Mahmoud, S. and Alwabli, A.S., 2017. An efficient hyperbolic shear deformation theory for bending, buckling and free vibration of FGM sandwich plates with various boundary conditions. *Steel and Composite Structures, 25*(6), pp.693-704.

[2] Asgari, M. and Akhlaghi, M., 2011. Natural frequency analysis of 2D-FGM thick hollow cylinder based on three-dimensional elasticity equations. *European Journal of Mechanics-A/Solids, 30*(2), pp.72-81.

[3] Dogan, V., 2013. Nonlinear vibration of FGM plates under random excitation. *Composite Structures, 95*, pp.366-374.

[4] Hadji, L. and Adda Bedia, E., 2015. Influence of the porosities on the free vibration of FGM beams. *Wind and structures, 21*(3), pp.273-287.

[5] Hadji, L., Khelifa, Z., Daouadji, T. and Bedia, E., 2015. Static bending and free vibration of FGM beam using an exponential shear deformation theory. *Coupled Systems Mechanics, 4*(1), pp.99-114.

[6] Kim, S.-E., Duc, N.D., Nam, V.H. and Van Sy, N., 2019. Nonlinear vibration and dynamic buckling of eccentrically oblique stiffened FGM plates resting on elastic foundations in thermal environment. *Thin-Walled Structures, 142*, pp.287-296.

[7] Mollarazi, H., Foroutan, M. and Moradi-Dastjerdi, R., 2012. Analysis of free vibration of functionally graded material (FGM) cylinders by a meshless method. *Journal of Composite Materials, 46*(5), pp.507-515.

[8] Pradhan, S. and Murmu, T., 2009. Thermo-mechanical vibration of FGM sandwich beam under variable elastic foundations using differential quadrature method. *Journal of Sound and Vibration, 321*(1-2), pp.342-362.

[9] Singh, S. and Harsha, S., 2020. Nonlinear vibration analysis of sigmoid functionally graded sandwich plate with ceramic-FGM-metal layers. *Journal of Vibration Engineering and Technologies, 8*(1), pp.67-84.

[10] Tang, Y. and Ding, Q., 2019. Nonlinear vibration analysis of a bi-directional functionally graded beam under hygro-thermal loads. *Composite Structures, 225*, p.111076.

[11] Yousfi, M., Atmane, H.A., Meradjah, M., Tounsi, A. and Bennai, R., 2018. Free vibration of FGM plates with porosity by a shear deformation theory with four variables. *Structural engineering and mechanics: An international journal, 66*(3), pp.353-368.

[12] Tang, Y. and Yang, T., 2018. Post-buckling behavior and nonlinear vibration analysis of a fluid-conveying pipe composed of functionally graded material. *Composite Structures, 185*, pp.393-400.

[13] Jha, D., Kant, T. and Singh, R., 2013. A critical review of recent research on functionally graded plates. *Composite Structures, 96*, pp.833-849.

[14] Jia, X., Yang, J. and Kitipornchai, S., Characterization of FGM micro-switches under electrostatic and casimir forces. IOP conference series: materials science and engineering, 2010. IOP Publishing, 012178.

[15] Jia, X., Yang, J., Kitipornchai, S. and Lim, C.W., 2010. Free vibration of geometrically nonlinear micro-switches under electrostatic and casimir forces. *Smart Materials and Structures, 19*(11), p.115028.

[16] Batra, R., Porfiri, M. and Spinello, D., 2008. Vibrations of narrow microbeams predeformed by an electric field. *Journal of Sound and Vibration, 309*(3-5), pp.600-612.

[17] Hasanyan, D., Batra, R. and Harutyunyan, S., 2008. Pull-in instabilities in functionally graded microthermoelectromechanical

systems. *Journal of Thermal Stresses, 31*(10), pp.1006-1021.

[18] Zhang, J. and Fu, Y., 2012. Pull-in analysis of electrically actuated viscoelastic microbeams based on a modified couple stress theory. *Meccanica, 47*(7), pp.1649-1658.

[19] Lee, Z., Ophus, C., Fischer, L., Nelson-Fitzpatrick, N., Westra, K., Evoy, S., Radmilovic, V., Dahmen, U. and Mitlin, D., 2006. Metallic nems components fabricated from nanocomposite al–mo films. *Nanotechnology, 17*(12), p.3063.

[20] Witvrouw, A. and Mehta, A., 2005. The use of functionally graded poly-sige layers for mems applications. *Materials science forum*, *492-493*. pp.255-260.

[21] Boutaleb, S., Benrahou, K.H., Bakora, A., Algarni, A., Bousahla, A.A., Tounsi, A., Tounsi, A. and Mahmoud, S., 2019. Dynamic analysis of nanosize FG rectangular plates based on simple nonlocal quasi 3d hsdt. *Advances in nano research, 7*(3), p.191.

[22] Chaht, F.L., Kaci, A., Houari, M.S.A., Tounsi, A., Bég, O.A. and Mahmoud, S., 2015. Bending and buckling analyses of functionally graded material (FGM) size-dependent nanoscale beams including the thickness stretching effect. *Steel and Composite Structures, 18*(2), pp.425-442.

[23] Liu, D., He, Y., Dunstan, D.J., Zhang, B., Gan, Z., Hu, P. and Ding, H., 2013. Toward a further understanding of size effects in the torsion of thin metal wires: An experimental and theoretical assessment. *International Journal of Plasticity, 41*, pp.30-52.

[24] Liu, D., He, Y., Tang, X., Ding, H., Hu, P. and Cao, P., 2012. Size effects in the torsion of microscale copper wires: Experiment and analysis. *Scripta Materialia, 66*(6), pp.406-409.

[25] Chong, A., Yang, F., Lam, D.C. and Tong, P., 2001. Torsion and bending of micron-scaled structures. *Journal of Materials Research, 16*(4), pp.1052-1058.

[26] Gurtin, M.E. and Murdoch, A.I., 1975. A continuum theory of elastic material surfaces. *Archive for rational mechanics and analysis, 57*(4), pp.291-323.

[27] Gurtin, M., Weissmüller, J. and Larche, F., 1998. A general theory of curved deformable interfaces in solids at equilibrium. *Philosophical Magazine A, 78*(5), pp.1093-1109.

[28] Eghbali, M. and Hosseini, S.A., 2022. Influences of magnetic environment and two moving loads on lateral and axial displacement of sandwich graphene-reinforced copper-based composite beams with soft porous core. *Journal of Vibration and Control*, p.10775463221135030.

[29] Eghbali, M. and Hosseini, S.A., 2023. On moving harmonic load and dynamic response of carbon nanotube-reinforced composite beams using higher-order shear deformation theories. *Mechanics Of Advanced Composite Structures, 10*(2), pp.257-270.

[30] Eghbali, M., Hosseini, S.A. and Hamidi, B.A., 2022. Mantari's higher-order shear deformation theory of sandwich beam with cntrc face layers with porous core under thermal loading. *International Journal of Structural Stability and Dynamics, 22*(16), p.2250181.

[31] Eghbali, M., Hosseini, S.A. and Pourseifi, M., 2022. Free transverse vibrations analysis of size-dependent cracked piezoelectric nano-beam based on the strain gradient theory under mechanic-electro forces. *Engineering Analysis with Boundary Elements, 143*, pp.606-612.

[32] Eghbali, M., Hosseini, S.A. and Pourseifi, M., 2022. An dynamical evaluation of size-dependent weakened nano-beam based on the nonlocal strain gradient theory. *The Journal of Strain Analysis for Engineering Design*, p.03093247221135210.

[33] Eghbali, M., Hosseini, S.A. and Rahmani, O., 2021. Free vibration of axially functionally graded nanobeam with an attached mass based on nonlocal strain gradient theory via new adm numerical method. *Amirkabir Journal Mechanical Engineering, 53*(2), pp.1159-1178.

[34] Bar On, B., Altus, E. and Tadmor, E.B., 2010. Surface effects in non-uniform nanobeams: Continuum vs. Atomistic modeling. *International Journal of Solids and Structures, 47*(9), pp.1243-1252.

[35] Wang, G.-F. and Feng, X.-Q., 2007. Effects of surface elasticity and residual surface tension on the natural frequency of microbeams. *Applied Physics Letters, 90*(23), p.231904.

[36] Ansari, R. and Sahmani, S., 2011. Bending behavior and buckling of nanobeams including surface stress effects corresponding to different beam theories.

International Journal of Engineering Science, 49(11), pp.1244-1255.

[37] Ansari, R., Mohammadi, V., Faghih Shojaei, M., Gholami, R. and Sahmani, S., 2014. Postbuckling analysis of timoshenko nanobeams including surface stress effect. *International Journal of Engineering Science, 75*, pp.1-10.

[38] Abbasion, S., Rafsanjani, A., Avazmohammadi, R. and Farshidianfar, A., 2009. Free vibration of microscaled timoshenko beams. *Applied Physics Letters, 95*(14), p.143122.

[39] Wang, L., 2010. Vibration analysis of fluid-conveying nanotubes with consideration of surface effects. *Physica E: Low-dimensional Systems and Nanostructures, 43*(1), pp.437-439.

[40] Farshi, B., Assadi, A. and Alinia-Ziazi, A., 2010. Frequency analysis of nanotubes with consideration of surface effects. *Applied Physics Letters, 96*(9), p.093105.

[41] He, J. and Lilley, C.M., 2008. Surface effect on the elastic behavior of static bending nanowires. *Nano letters, 8*(7), pp.1798-1802.

[42] Civalek, Ö., Uzun, B. and Yaylı, M.Ö., 2022. An effective analytical method for buckling solutions of a restrained FGM nonlocal beam. *Computational and Applied Mathematics, 41*(2), pp.67.

[43] Uzun, B. and Yaylı, M.Ö., 2023. Stability analysis of arbitrary restrained nanobeam embedded in an elastic medium via nonlocal strain gradient theory. *The Journal of Strain Analysis for Engineering Design*, p.03093247231164261.

[44] Nazemnezhad, R., Salimi, M., Hosseini Hashemi, S. and Asgharifard Sharabiani, P., 2012. An analytical study on the nonlinear free vibration of nanoscale beams incorporating surface density effects. *Composites Part B: Engineering, 43*(8), pp.2893-2897.

[45] Ansari, R., Mohammadi, V., Shojaei, M.F., Gholami, R. and Rouhi, H., 2014. Nonlinear vibration analysis of timoshenko nanobeams based on surface stress elasticity theory. *European Journal of Mechanics-A/Solids, 45*, pp.143-152.

[46] Asgharifard Sharabiani, P. and Haeri Yazdi, M.R., 2013. Nonlinear free vibrations of functionally graded nanobeams with surface effects. *Composites Part B: Engineering, 45*(1), pp.581-586.

[47] Yayli, M.Ö., 2016. Buckling analysis of a microbeam embedded in an elastic medium with deformable boundary conditions. *Micro and Nano Letters, 11*(11), pp.741-745.

[48] Yayli, M.Ö., 2018. Free longitudinal vibration of a nanorod with elastic spring boundary conditions made of functionally graded material. *Micro and Nano Letters, 13*(7), pp.1031-1035.

[49] Yayli, M.Ö., 2018. Free vibration analysis of a single-walled carbon nanotube embedded in an elastic matrix under rotational restraints. *Micro and Nano Letters, 13*(2), pp.202-206.

[50] Yayli, M.Ö., 2019. Effects of rotational restraints on the thermal buckling of carbon nanotube. *Micro and Nano Letters, 14*(2), pp.158-162.

[51] Yayli, M.Ö., 2019. Free vibration analysis of a rotationally restrained (FG) nanotube. *Microsystem Technologies, 25*(10), pp.3723-3734.

[52] Yayli, M.Ö., 2020. Axial vibration analysis of a rayleigh nanorod with deformable boundaries. *Microsystem Technologies, 26*(8), pp.2661-2671.

[53] Yaylı, M.Ö., 2015. Buckling analysis of a rotationally restrained single walled carbon nanotube. *Acta Physica Polonica A*.

[54] Lim, C.W., Li, C. and Yu, J.L., 2012. Free torsional vibration of nanotubes based on nonlocal stress theory. *Journal of Sound and Vibration, 331*(12), pp.2798-2808.

[55] Li, L. and Hu, Y., 2017. Torsional vibration of bi-directional functionally graded nanotubes based on nonlocal elasticity theory. *Composite Structures, 172*, pp.242-250.

[56] Murmu, T., Adhikari, S. and Wang, C., 2011. Torsional vibration of carbon nanotube–buckyball systems based on nonlocal elasticity theory. *Physica E: Low-dimensional Systems and Nanostructures, 43*(6), pp.1276-1280.

[57] Civalek, O., Uzun, B. and Yayli, M.O., 2022. A fourier sine series solution of static and dynamic response of nano/micro-scaled fg rod under torsional effect. *Advances in nano research, 12*(5), pp.467-482.

[58] Uzun, B. and Yaylı, M.Ö., 2022. Porosity dependent torsional vibrations of restrained fg nanotubes using modified couple stress theory. *Materials Today Communications, 32*, p.103969.

[59] Nazemnezhad, R. and Fahimi, P., 2017. Free torsional vibration of cracked nanobeams

incorporating surface energy effects. *Applied Mathematics and Mechanics, 38*(2), pp.217-230.

[60] Nazemnezhad, R., Mehrianpoor, R. and Jandaghian, A.A., 2023. Internal resonances of nanorods in presence of surface energy effect: Nonlinear torsional vibration. *Mathematics and Mechanics of Solids, 28*(3), pp.833-853.

[61] Uzun, B., Civalek, Ö. and Yaylı, M.Ö., 2022. Axial and torsional free vibrations of restrained single-walled boron nitride nanotube (swbnnt) embedded in an elastic medium via nonlocal strain gradient theory. *Waves in Random and Complex Media*, doi.org/10.1080/17455030.2022.2147600.

[62] Uzun, B., Civalek, Ö. and Yaylı, M.Ö., 2023. Torsional and axial vibration of restrained saturated nanorods via strain gradient elasticity. *Archive of Applied Mechanics, 93*(4), pp.1605-1630.

[63] Yayli, M.Ö., 2018. Torsional vibration analysis of nanorods with elastic torsional restraints using non-local elasticity theory. *Micro and Nano Letters, 13*(5), pp.595-599.

[64] Rao, S.S., 2007. *Vibration of continuous systems*. Wiley Online Library.

[65] Gheshlaghi, B. and Hasheminejad, S.M., 2010. Size dependent torsional vibration of nanotubes. *Physica E: Low-dimensional Systems and Nanostructures, 43*(1), pp.45-48.

[66] Gurtin, M.E. and Ian Murdoch, A., 1975. A continuum theory of elastic material surfaces. *Archive for Rational Mechanics and Analysis, 57*(4), pp.291-323.

[67] Gurtin, M.E., Weissmüller, J. and Larché, F., 1998. A general theory of curved deformable interfaces in solids at equilibrium. *Philosophical Magazine A, 78*(5), pp.1093-1109.

[68] Setoodeh, A.R., Rezaei, M. and Zendehdel Shahri, M.R., 2016. Linear and nonlinear torsional free vibration of functionally graded micro/nano-tubes based on modified couple stress theory. *Applied Mathematics and Mechanics, 37*(6), pp.725-740.